DEM-assisted in-season soil moisture estimation based on normalized Sentinel-1 SAR imagery

Gregoriy Kaplan*[1,2], Michael Gross[2], Itamar Michel-Meyer[2], Matan Rahav[2], Guy Sela[2.3]

[1]Terra Space Lab, Tel Aviv, Israel

[2] CropX, Natanya, Israel

[3] yieldsApp, Israel

*Corresponding author. Email: gregoriy@terraspacelab.com

DEM-assisted in-season soil moisture estimation based on normalized Sentinel-1 SAR imagery

Gregoriy Kaplan*[1,2], Michael Gross[2], Itamar Michel-Meyer[2], Matan Rahav[2], Guy Sela[2.3]

[1]Terra Space Lab, Tel Aviv, Israel

[2] CropX, Natanya, Israel

[3] yieldsApp, Israel

*Corresponding author. Email: gregoriy@terraspacelab.com

Abstract

Soil moisture is a crucial in-field variable used in many applications. Soil moisture might be measured in the field using soil sensors and can be estimated via satellite imagery. The present study proposes an innovative SAR-based method that significantly improves the accuracy of soil moisture estimation and does not require field-measured data. The method is based on the previously developed SAR local incidence angle normalization method and utilizes a newly developed equation, which takes a digital elevation model DEM into account. The volumetric water content (VWC) measurements were recorded at depths of 20 and 46 cm on 10 alfalfa fields in the US by 37 soil sensors. Recorded VWC data was correlated to the average field values of SAR imagery processed by the proposed method. The developed models have the following statistical performance: R^2 = 0.5616 with RMSE = 3.9758 for VWC at 20 cm and R^2 = 0.4247 with RMSE = 4.0133 for VWC at 46 cm. In both cases, the improvement of R^2 of models based on the proposed method over models based on SAR imagery, which were not processed by the new method, was significant.

Keywords: SAR, Sentinel-1, Soil moisture, DEM, Copernicus 30.

1. Introduction

Estimation of the in-field soil moisture is a crucial task, especially during the growing season, because it is used for many applications such as defining the irrigation dose [1]. In-field soil moisture measurements are possible to take directly using field sensors. This technology requires manual labour and demands the installation of a large number of sensors because each sensor provides only local measurements. To mitigate these drawbacks various satellite-based soil moisture estimation methods were developed. These methods might be optical-based [2,3], based on the Synthetic Aperture Radar (SAR) imagery [4,5], and combined including optical and SAR

[6], as well as optical and GNSS-R [7]. The main advantage of the SAR imagery over optical is the cloud penetration ability [8]. Previously, a large number of various SAR based soil moisture algorithms and models was developed [9]. Despite the advantages of these methods, the majority of previously developed approaches, including the commonly-used Oh and Dubois models are applicable mostly to bare soils, require field data related to soil roughness and composition, calibration and validation of coefficients used by the models [5,10–13].

The present article suggests a new method of in-season soil moisture estimation based on Sentinel-1 SAR imagery. The proposed method is built upon the effective local incidence angle normalization and adds a newly-developed equation, which uses a digital elevation model (DEM) to perform additional radiometric normalization. The main advantage of the new method is that it does not require any field-measured data and prior knowledge.

2. Material and Methods

2.1.Study site and field Measurements

The study sites are located in two areas in Arizona, US. Overall, 8 alfalfa fields are located in the Northern area near the city of Maricopa, and 2 alfalfa fields are located in the Southern site near Santa Rosa (Fig 1).

The field campaign took place between 30 August 2021 and 29 December 2021. During that time volumetric water content (VWC) values, which is a quantitative representation of soil moisture, were recorded on the depths of 20 and 46 cm in fields by soil moisture sensors (CropX, Israel [14]) with the accuracy of approximately 1%. Overall, 37 sensors were installed in the fields (3-4 sensors per field). The SAR imagery and VWC field measurements in all fields were obtained both in bare soil (up to approximately middle of September 2021 at same fields) and vegetated field conditions including the full development of the vegetation. Fig. 2. shows the NDVI [15] curves derived for the fields using available optical Sentinel-2 imagery. NDVI despite its limitations is the vegetation index used most commonly as proxy of vegetation development [16].

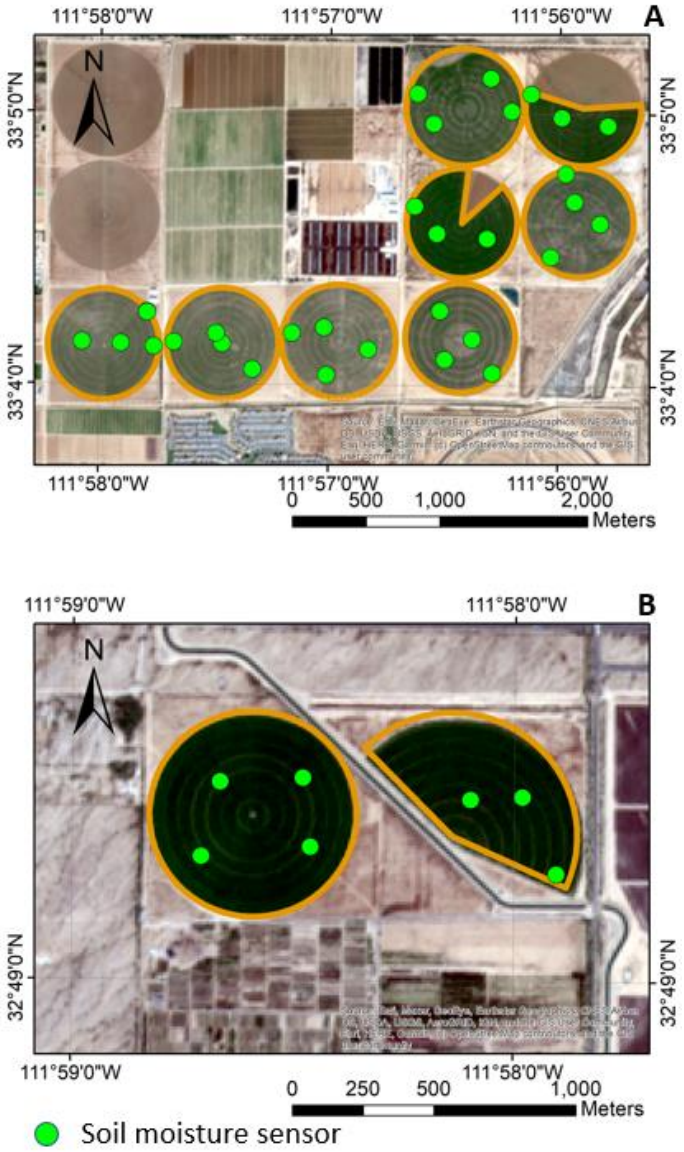

Fig 1. Study sites: A) Maricopa alfalfa fields; B) Santa Rosa alfalfa fields. Basemap: Sentinel-2 images acquired 10 November 2021.

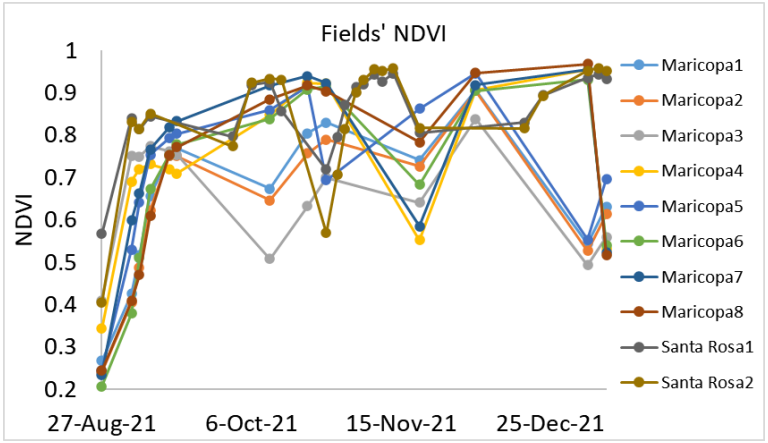

Fig. 2. Sentinel-2 NDVI curves corresponding to the vegetation development in 10 alfalfa fields used in the study.

The statistical data representing sizes of fields and standard deviations of elevation within fields (derived from Copernicus 30 DEM) are presented in Table 1.

Table 1. Area (in Sentinel-1 GRD pixel size) and standard deviation of pixels' elevation of the 10 fields used in the study.

Field	Area (Sentinel-1 10*10m Pixels)	St.Dev (m)
Maricopa 1	5356	0.43
Maricopa 2	5399	0.47
Maricopa 3	5639	0.44
Maricopa 4	5203	0.79
Maricopa 5	4697	0.89
Maricopa 6	5950	0.78
Maricopa 7	5209	1.07
Maricopa 8	3223	1.12
Santa Rosa 1	3197	1.02
Santa Rosa 2	4988	1.74
Min	3197	0.43
Max	5950	1.74
Average	4886	0.87

2.2 . SAR imagery and SAR image processing

Sentinel-1 is a constellation of two satellites equipped with C-band synthetic aperture phased array [17] radar working VV and VH polarizations on a wavelength of approximately 5.55 cm which permits low attenuation in the atmosphere [18]. The resolution of the Level-1 Ground Range Detected (GRD) Interferometric Wide (IW) mode used in this study is 20 × 22 m, with a pixel size of 10 × 10 m, a swath width of 250 km, and a revisit time of six days for images with the same geometry. Sentinel-1A and Sentinel-1B were launched on 3 April 2014 and on 25 April 2016, respectively. Unfortunately, on 23 December 2021, Sentinel-1B suffered a failure and stopped providing new imagery. Overall, 52 SAR images acquired from 30 August 2021 to 29 December 2021 were used in the present study. The local incidence angles range of the used SAR images is 33.8°-45.3°

All Sentinel-1 images were pre-processed in the Sentinel Application Platform (SNAP version 8.0, European Space Agency). The sequential pre-processing of the Sentinel-1 imagery was as follows: subsetting a region around the target area, applying the latest orbit file to correct for the satellite path, thermal noise removal, calibration to σ^0 in a natural scale, range-Doppler terrain correction using the Copernicus 30 digital elevation model. Afterwards, the SAR imagery was normalized to compensate for the negative effect of the difference of local incidence angles between

SAR images in the time series [19,20]. The normalization was done using the previously developed methodology [21].

$$\sigma^0_{Norm} = \sigma^0 * \theta \quad (1),$$

Where σ^0 is radar cross-section per unit area [22] in linear scale at VH or VV polarization, θ – local incidence angle. It is important to note that all available imagery were acquired at all available incidence angles on both ascending and descending orbits.

After that, each normalized σ^0 value was smoothed (i.e. radiometrically normalized) to mitigate the SAR backscatter dependence of the local relief [18,20] by dividing the σ^0_{Norm} by the standard deviation of average elevation values (in meters) of the field. The elevation values of the field were based on the Copernicus 30 DEM, which is the more accurate representation of the Earth's surface than the SRTM [23] and other commonly used DEMs [24]:

$$\sigma^0_{Norm,smooth} = \sigma^0_{Norm}/StDev_{elevation} \quad (2),$$

2.3. Model development and validation

While the direct estimation of soil moisture on the depth of 46 cm and even 20 cm is not possible via C-band SAR in most cases [20,25], the present study exploits the existing relationship between the top-soil moisture and the soil moisture on the deeper levels [2]. Owing to this knowledge average in-polygon VWC values recorded at the depths of 20 cm and 46 cm by CropX sensors in the fields at the time most close to the time of image acquisition were correlated to the SAR backscatter values. In most cases, the time difference between sensors measurements and image acquisition times was in the range of 2-3 minutes.

Correlation between $\sigma^0_{Norm,smooth}$ and VWC values averaged for each field using data recorded by the sensors installed in the fields, was found using polynomial models. The following SAR image processing algorithm was used for deriving two separate models for estimation of VWC at 20 cm and VWC at 46 cm:

$$\sigma^0_{Norm,smooth,VH} + \sigma^0_{Norm,smooth,VV} \quad (3),$$

VWC 20 and VWC 46 estimation models based on $\sigma^0_{Norm,smooth}$ were compared to models based on σ^0 values that were not normalized and smoothed:

$$\sigma^0_{VH} + \sigma^0_{VV} \quad (4),$$

In each model, 416 data points representing SAR backscatter and corresponding field measured VWC values were used.

The commonly used [21,26] Steiger variation [27] of the two-tailed Fisher Z-score tests [28] was performed to determine whether the difference in both types (based on $\sigma^0_{Norm,smooth}$ and based on σ^0) of models' R^2 is significant ($\alpha \leq 0.05$).

Apart from estimating the correlation between processed SAR imagery and in-field VWC, the correlation between measured VWC at 20 cm and VWC at 46 cm was found.

3. Results and Discussion

Table 1 shows in-field average VWC at 20 cm and VWC at 46 cm values that were recorded at the time closest to the times of SAR imagery acquisition during the period used for deriving the models.

Table 1. Statistics of VWC 20 and VWC 46 data used in the study.

	VWC 20 (%)	VWC 46 (%)
Min	4.6	7.4
Max	36.6	31.4
Average	20.0	22.0

The statistics of VWC at 20 cm and VWC at 46 cm estimation models based on σ^0 and $\sigma^0_{Norm,smooth}$ (Fig. 3.) alongside the difference in R^2 and RMSE between two types of models are provided in Table 2. Following normalization and smoothing procedures R^2 and RMSE were improved by 0.4767 and 30.79% for VWC at 20 cm and 0.3604 and 22.47% for VWC at 46 cm. In both cases, the improvement of R^2 was statistically significant with $p = 0$.

Table 2. Statistics of SAR-based VWC 20 and VWC 46 estimation models.

	VWC 20 cm	VWC 46 cm
R^2 $\sigma^0_{VH} + \sigma^0_{VH}$	0.0849	0.0645
RMSE $\sigma^0_{VH} + \sigma^0_{VH}$	5.7446	5.1767
R^2 $\sigma^0_{Norm,smooth,VH} + \sigma^0_{Norm,smooth,VV}$	0.5616	0.4247
RMSE $\sigma^0_{Norm,smooth,VH} + \sigma^0_{Norm,smooth,VV}$	3.9758	4.0133
R^2 improvement	0.4767	0.3602
RMSE improvement (%)	1.7688 (30.79%)	1.1634 (22.47%)
Models' R^2 Z	12.504	10.258
Models' R^2 p	0	0

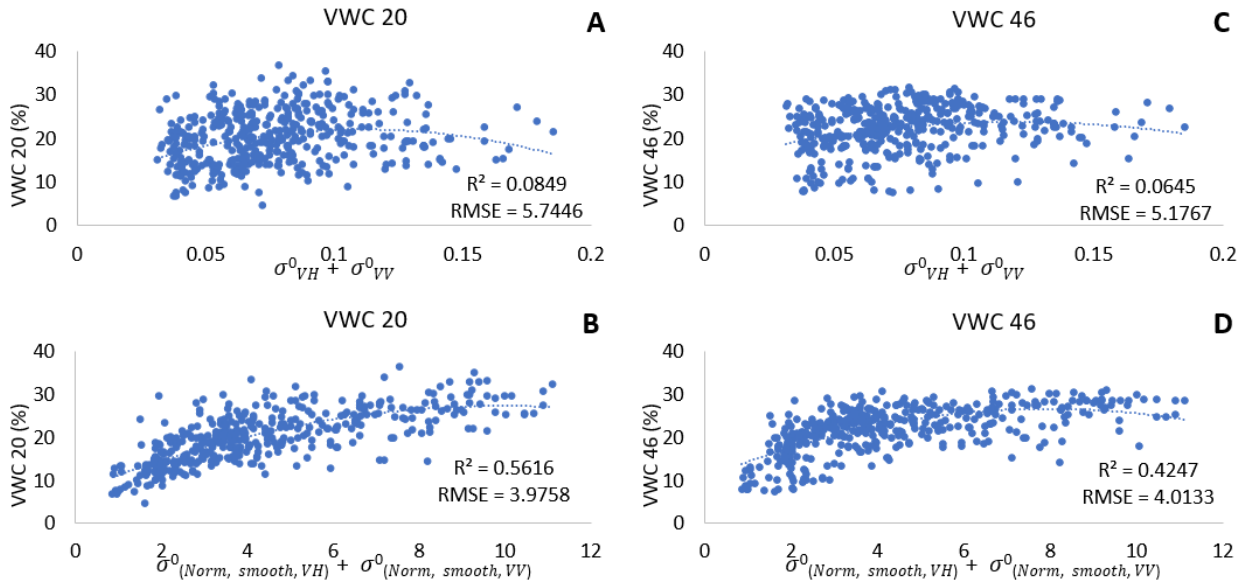

Fig. 3. VWC 20 and VWC 46 SAR-based estimation models: A) $\sigma^0_{VH} + \sigma^0_{VH}$ VWC 20; B) $\sigma^0_{VH} + \sigma^0_{VH}$ VWC 46; C) $\sigma^0_{Norm,smooth,VH} + \sigma^0_{Norm,smooth,VV}$ VWC 20; D) $\sigma^0_{Norm,smooth,VH} + \sigma^0_{Norm,smooth,VV}$ VWC 46.

Measured VWC at 20 cm showed a correlation with VWC at 46 cm with $R^2 = 0.6745$ with RMSE = 3.3848 (Fig. 4).

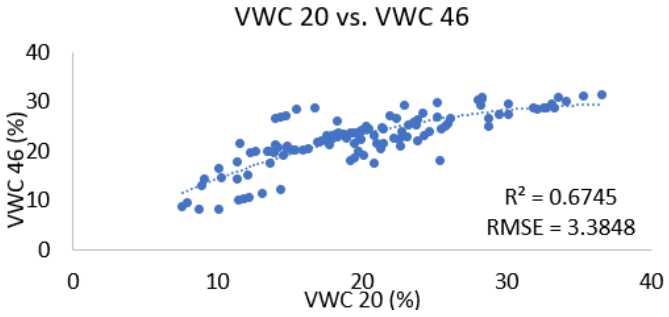

Fig. 4. Correlation between field measured VWC at 20 and 46 cm.

It should be noted that models developed in the present study showed their performance during both bare soil conditions and in the estimation of the VWC in fields covered by vegetation. Importantly, the application of the suggested methodolodgy does not require ground-measured data and any prior knowledge about a field. The present study was conducted on 10 alfalfa fields and similar approaches might be applicable to soil moisture estimation in the fields covered with other crops, but additional studies should be performed in order to confirm this assumption.

4. Conclusions

The present study found a correlation between processed SAR imagery and soil moisture measured at two depths (20 and 46 cm). Importantly, the correlation significantly improved after local incidence angle normalization and innovative smoothing procedures were applied. Therefore, the present study confirmed the effectiveness of the local incidence angle normalization method [21] and showed the potential of the newly-developed smoothing method in soil moisture estimation. The study also found a good correlation between soil moisture (VWC values) measured at depths of 20 and 46 cm.

Author Contributions: Conceptualization, G.K., M.G., I. M.-M., M.R., G.S; methodology, G.K.; software, G.K., M.G., I.M.-M.; formal analysis, G.K., M.G.; investigation, G.K.; fieldwork, M.G.; writing—original draft preparation, G.K.; writing—review and editing, G.K., M.G., I. M.-M., M.R., G.S; visualization, G.K.; supervision, G.S.; project administration, G.S.; funding acquisition, G.S., M.R. All authors have read and agreed to the published version of the manuscript.

Funding: This work was financed by the CropX LTD.

Competing interests: The authors declare that there is no conflict of interest regarding the publication of this article.

References

1. Ihuoma, S.O.; Madramootoo, C.A.; Kalacska, M. Integration of satellite imagery and in situ soil moisture data for estimating irrigation water requirements. *Int. J. Appl. Earth Obs. Geoinf.* **2021**, *102*, 102396, doi:10.1016/j.jag.2021.102396.

2. Rijal, S.; Zhang, X.; Jia, X. Estimating Surface Soil Water Content in the Red River Valley of the North using Landsat 5 TM Data. *Soil Sci. Soc. Am. J.* **2013**, *77*, 1133–1143, doi:10.2136/sssaj2012.0295.

3. Sedaghat, A.; Shahrestani, M.S.; Noroozi, A.A.; Fallah Nosratabad, A.; Bayat, H. Developing pedotransfer functions using Sentinel-2 satellite spectral indices and Machine learning for estimating the surface soil moisture. *J. Hydrol.* **2022**, *606*, 127423, doi:10.1016/j.jhydrol.2021.127423.

4. Kaplan, G.; Gross, M.; Badakhova, G.K. Estimation of cotton field variables

using Sentinel-1 SAR imagery levelling algorithm. *Sci. Herit.* **2021**, *2*, 6–9, doi:10.24412/9215-0365-2021-79-2-6-9.

5. Chung, J.; Lee, Y.; Kim, J.; Jung, C.; Kim, S. Soil Moisture Content Estimation Based on Sentinel-1 SAR Imagery Using an Artificial Neural Network and Hydrological Components. *Remote Sens.* **2022**, *14*, 465, doi:10.3390/rs14030465.

6. Wang, Q.; Li, J.; Jin, T.; Chang, X.; Zhu, Y.; Li, Y.; Sun, J.; Li, D. Comparative Analysis of Landsat-8, Sentinel-2, and GF-1 Data for Retrieving Soil Moisture over Wheat Farmlands. *Remote Sens.* **2020**, *12*, 2708, doi:10.3390/rs12172708.

7. Sánchez, N.; Alonso-Arroyo, A.; Martínez-Fernández, J.; Piles, M.; González-Zamora, Á.; Camps, A.; Vall-llosera, M. On the Synergy of Airborne GNSS-R and Landsat 8 for Soil Moisture Estimation. *Remote Sens.* **2015**, *7*, 9954–9974, doi:10.3390/rs70809954.

8. Reamer, R.E.; Stockton, W.O.; Stromfors, R.D. New military uses for Synthetic Aperture Radar (SAR). *Airborne Reconnaiss. XVI* **1993**, 113–119, doi:doi:10.1117/12.140829.

9. Petropoulos, G.P.; Ireland, G.; Barrett, B. Surface soil moisture retrievals from remote sensing: Current status, products & future trends. *Phys. Chem. Earth* **2015**, *83–84*, 36–56, doi:10.1016/j.pce.2015.02.009.

10. Ayari, E.; Kassouk, Z.; Lili-Chabaane, Z.; Baghdadi, N.; Bousbih, S.; Zribi, M. Cereal Crops Soil Parameters Retrieval Using L-Band ALOS-2 and C-Band Sentinel-1 Sensors. *Remote Sens.* **2021**, *13*, 1393, doi:10.3390/rs13071393.

11. Baghdadi, N.; Choker, M.; Zribi, M.; El Hajj, M.; Paloscia, S.; Verhoest, N.E.C.; Lievens, H.; Baup, F.; Mattia, F. A new empirical model for radar scattering from bare soil surfaces. *Remote Sens.* **2016**, *8*, 1–14, doi:10.3390/rs8110920.

12. Zheng, X.; Feng, Z.; Li, L.; Li, B.; Jiang, T.; Li, X.; Li, X.; Chen, S. Simultaneously estimating surface soil moisture and roughness of bare soils by combining optical and radar data. *Int. J. Appl. Earth Obs. Geoinf.* **2021**, *100*, 102345, doi:10.1016/j.jag.2021.102345.

13. Choker, M.; Baghdadi, N.; Zribi, M.; El Hajj, M.; Paloscia, S.; Verhoest, N.E.C.; Lievens, H.; Mattia, F. Evaluation of the Oh, Dubois and IEM backscatter models using a large dataset of SAR data and experimental soil measurements. *Water (Switzerland)*

2017, *9*, 38, doi:10.3390/w9010038.

14. Kaplan, G.; Gross, M.; Badakhova, G. New Sentinel-1 SAR imagery processing algorithm improves the estimation of cotton water consumption and field soil moisture. In Proceedings of the Hydrometeorology, climate change and environmental monitoring: current problems and ways of their solution; Tashkent, Uzbekistan, 2021; pp. 19–21.

15. Tucker, C.J. Red and photographic infrared linear combinations for monitoring vegetation. *Remote Sens. Environ.* **1979**, *8*, 127–150, doi:https://doi.org/10.1016/0034-4257(79)90013-0.

16. Kaplan, G.; Rozenstein, O. Spaceborne Estimation of Leaf Area Index in Cotton, Tomato, and Wheat Using Sentinel-2. *Land* **2021**, *10*, 505, doi:10.3390/land10050505.

17. Fenn, A.J. *Adaptive Antennas and Phased Arrays for Radar and Communications*; Artech House, 2008; ISBN 9781596932739.

18. Skolnik, M. *Radar Handbook. Third Edition*; McGraw-Hill, 2008; ISBN 978-0-07-148547-0.

19. Arias, M.; Campo-Bescós, M.Á.; Álvarez-Mozos, J. On the influence of acquisition geometry in backscatter time series over wheat. *Int. J. Appl. Earth Obs. Geoinf.* **2022**, *106*, 102671, doi:10.1016/j.jag.2021.102671.

20. Carver, K.R.; Elachi, C.; Ulaby, F.T. Microwave remote sensing from space. *Proc. IEEE* **1985**, *73*, 970–996, doi:10.1109/PROC.1985.13230.

21. Kaplan, G.; Fine, L.; Lukyanov, V.; Manivasagam, V.S.; Tanny, J.; Rozenstein, O. Normalizing the Local Incidence Angle in Sentinel-1 Imagery to Improve Leaf Area Index, Vegetation Height, and Crop Coefficient Estimations. *Land* **2021**, *10*, 680, doi:10.3390/land10070680.

22. Frey, O.; Santoro, M.; Werner, C.L.; Wegmuller, U. DEM-Based SAR Pixel-Area Estimation for Enhanced Geocoding Refinement and Radiometric Normalization. *IEEE Geosci. Remote Sens. Lett.* **2013**, *10*, 48–52, doi:10.1109/LGRS.2012.2192093.

23. Farr, T.G.; Rosen, P.A.; Caro, E.; Crippen, R.; Duren, R.; Hensley, S.; Kobrick, M.; Paller, M.; Rodriguez, E.; Roth, L.; et al. The Shuttle Radar Topography Mission. *Rev. Geophys.* **2007**, *45*, 44, doi:10.1029/2005RG000183.

24. Marešová, J.; Gdulová, K.; Pracná, P.; Moravec, D.; Gábor, L.; Prošek, J.; Barták, V.; Moudrý, V. Applicability of Data Acquisition Characteristics to the Identification of Local Artefacts in Global Digital Elevation Models: Comparison of the Copernicus and TanDEM-X DEMs. *Remote Sens.* **2021**, *13*, 3931, doi:10.3390/rs13193931.

25. Nolan, M.; Fatland, D.R. Penetration depth as a DInSAR observable and proxy for soil moisture. *IEEE Trans. Geosci. Remote Sens.* **2003**, *41*, 532–537, doi:10.1109/TGRS.2003.809931.

26. Kaplan, G.; Fine, L.; Lukyanov, V.; Manivasagam, V.S.; Malachy, N.; Tanny, J.; Rozenstein, O. Estimating Processing Tomato Water Consumption, Leaf Area Index, and Height Using Sentinel-2 and VENµS Imagery. *Remote Sens.* **2021**, *13*, 1046, doi:10.3390/rs13061046.

27. Steiger, J.H. Tests for comparing elements of a correlation matrix. *Psychol. Bull.* **1980**, *87*, 245–251.

28. Fisher, R.A. *On the Probable Error of a Coefficient of Correlation Deduced from a Small Sample*; Metron, 1921; Vol. 1;.